DNA Is a Template for Accelerating the Aggregation of Copper, Zinc Superoxide Dismutase[†]

Wei Jiang,[‡] Yingchun Han,[‡] Ruoyu Zhou,[‡] Lina Zhang,[‡] and Changlin Liu*[,§]

Department of Chemistry, Huazhong University of Science and Technology, Wuhan 430074, China, and Key Laboratory of Pesticide & Chemical Biology, Ministry of Education, Central China Normal University, Wuhan 430079, China

Received October 27, 2006; Revised Manuscript Received January 31, 2007

ABSTRACT: The proteinaceous aggregates rich in copper, zinc superoxide dismutase (SOD1) have been shown to be involved in pathogenesis of amyotrophic lateral sclerosis (ALS). Since negatively charged species such as nucleic acids have frequently been found associated with the proteinaceous deposits in the tissues of patients with amyloid diseases, we examined here the aggregation behavior of SOD1 in the presence of DNA under acidic conditions that facilitate protein aggregation. Several forms of double-stranded DNA were tested to trigger SOD1 aggregation by light scattering, single- and double-fluorescence imaging with dyes, atomic force microscopy, and direct observations under visible light. The results reveal that DNA acts as a template for accelerating the formation of SOD1 aggregates and is incorporated into SOD1 aggregates. The spherical and ellipsoidal SOD1 aggregates were characterized in both hydrated and dried states and have morphology similar to those identified in the diseased neurons. Light scattering experiments indicate that the aggregation first undergoes a rapid phase where the aggregates with average diameters of 40−80 nm rapidly form in <2 min, and then passes through a slow phase where the average diameters of aggregates were increased to at least 200−260 nm in 2 h. All forms of DNAs tested can lead to the aggregation of SOD1 at nanomolar levels. The association of SOD1 with DNA, driven by electrostatic interactions between both, can restrict the orientation of SOD1 molecules and increase a SOD1 population along DNA strands. This facilitates the hydrophobic interactions between SOD1 molecules, as indicated by hydrophobic probe binding and chemical denaturant treatment experiments. Demonstration of the DNA-accelerated aggregation of SOD1 might establish a possible role of DNA in the pathogenesis of some diseases because of the ubiquitous expression of SOD1 and the coexistence of SOD1 and DNA in the crowded molecular environment of a cell.

It is well-known that the primary function of wild type Cu,Zn superoxide dismutase (SOD1[1]) is to lower the steady-state concentration of the superoxide anion as an antioxidant enzyme. The enzyme is found in the cytosol, nucleus, peroxisomes, lysosomes, and mitochondrial intermembrane space as a homodimeric enzyme of ∼32 kDa containing one copper and one zinc per subunit (*1*). However, the mutations of SOD1 create unfavorable effects. It has been found that SOD1 involves development of amyotrophic lateral sclerosis (ALS), and causes motor neuron death through an as-yet unidentified molecular mechanism (*2*−*11*). Although it is well-established that the SOD1-mediated toxicity in diseases is not due to loss of function but instead due to a gain of one or more injurious properties that are independent of the levels of SOD activity, little is currently known about the roles of SOD1 in neurocytotoxicity (*6*, *7*, *12*, *13*).

Over 100 different mutations have been identified in the *sod1* genes of patients diagnosed with the familial form of ALS (fALS). These mutations result in a highly diverse group of mutant proteins, some of them very similar to and others enormously different from wild-type SOD1. Recent studies of fALS mutant SOD1 proteins suggest that the mutants partition into two groups with distinctly different biophysical characteristics with respect to metal content, SOD activity, and spectroscopy (*2*−*5*). These two groups have been termed metal-binding region (MBR) and wild-type-like (WTL) fALS mutant SOD1 proteins on the basis of their SOD activities and metal-binding properties (*2*−*5*). The MBR subset of SOD1 proteins has mutations that are localized in and around the metal-binding sites, including the electrostatic and zinc loops, and was found to have significantly altered metal-binding properties relative to wild-type SOD1. Two predominant models, including the abnormal aggregation or inclusion of SOD1 and aberrant copper-mediated oxidation chemistry in the misfolded enzymes, have been proposed to support the assumption that the toxicity of fALS mutant SOD1 proteins may induce motor neuron death and ALS (*6*−*19*).

[†] This work was supported by NSFC (Grant 20571028).

* To whom correspondence should be addressed. Fax: 86-27-87543632. E-mail: liuchl@mail.hust.edu.cn.

[‡] Huazhong University of Science and Technology.

[§] Central China Normal University.

[1] Abbreviations: Aβ, amyloid β peptides; AFM, atomic force microscopy; ALS, amyotrophic lateral sclerosis; ANS, 8-anilino-1-naphthalene-sulfonic acid; ctDNA, calf thymus DNA; DLS, dynamic light scattering; dsDNA, double-stranded DNA fragment; EtBr, ethidium bromide; fALS, familial amyotrophic lateral sclerosis; GdmCl, guanidinium chloride; GG, GeneGreen; MBR, metal-binding region; RALS, right angle light scattering; PrP, cellular prion protein; SOD1, copper, zinc superoxide dismutase; ThS, thioflavin S; WTL, wild-type-like.

10.1021/bi062234m CCC: $37.00 © 2007 American Chemical Society
Published on Web 05/01/2007

The aggregation hypothesis maintains that mutant SOD1 proteins are or become misfolded and consequently oligomerize into high-molecular-weight species that ultimately aggregate and end up in proteinaceous inclusions (*20*). Proteinaceous aggregates rich in SOD1 have been found in tissues from ALS patients, ALS-SOD1 transgenic mice, and in cell culture models, leading to the conclusion that SOD1-associated familial ALS is a protein conformational disorder, similar to other neurodegenerative diseases in which protein aggregates are found (*21*). High-molecular-weight oligomerized species of SOD1, which may be more closely related to the toxic form, are found in the spinal cords of mice expressing mutant SOD1 well before disease onset or the appearance of the much larger microscopically visible fibrils or inclusions (*22*−*24*). The visible aggregates or inclusions in SOD1-linked diseases contain neurofilament proteins, ubiquitin, and covalent adducts to other components in addition to SOD1, but it is not known if copper, zinc, or any other metal ions and any other components including lipids and nucleic acids are involved in their formation (*6*, *7*). The aggregation of SOD1 is a complex multistep process that consists of dimer dissociation, loss of metals, conformation changes, nucleation, and accretion, and involves many components (*25*). Perturbing the environmental conditions, such as lowering pH, adding metal chelator, disulfide linkage reduction, and oxidative modification, can help us understand the formation processes of protein aggregates (*26*−*28*).

Although protein aggregation may be a common feature of SOD1-mediated toxicity, to date the ultimate mechanisms underlying the SOD1-mediated cytotoxicity are still unknown, despite years of intensive study (*6*, *7*, *12*, *13*). Aggregates are clearly identifiable, but thus far have not been directly linked to any of the disruptions in cellular functions and could be protective rather than pathogenic (*6*, *7*). The oxidation chemistry might be only one of the chemical steps occurring in the SOD1 aggregation. Perhaps SOD1 might possess some unknown properties that cause the injurious effects (*7*). In this study, we examined the propensity of SOD1 to aggregate in acidic solutions (pH 3.6) upon addition of DNA, a phenomenon that we have noted during observation of the SOD1-mediated DNA hydrolytic cleavage activity (*29*, *30*), based on the following considerations. First, since lowering pH can also compromise the metal-binding properties and lead to loss of metals like the MBR mutants, the aggregation behavior of SOD1 occurring under acidic conditions could mimic the effect of mutations and reflect the practical process done under physiological conditions to a high extent (*26*, *28*). Second, X-ray structure determination has shown that some of the fALS SOD1 mutants form a highly ordered structure that is an amyloid-like linear or helical filament, or a water-filled nanotube with an outside diameter of ∼9 nm and an inside diameter of ∼3 nm (*31*−*33*). DNA might be sequestered within the aggregate structure due to matched sizes. The coexistence of SOD1 up to 40 μM (*34*) and DNA in the cellular crowded environments can assist SOD1 binding to DNA (*35*). Third, a complete composition of SOD1 aggregates observed in a variety of in vivo models remains to be examined (*7*, *8*, *12*, *17*, *18*, *24*, *36*−*38*), and the involvement of DNA in the aggregation of SOD1 cannot be ruled out. Indeed, in the brain tissue from victims of Alzheimer's disease, nucleic acids have been detected in senile plaques composed of the Aβ peptides (*39*). Fourth, the observation that long-chain unsaturated fatty acids induce the formation of high-molecular-weight aggregates containing SOD1 under neutral conditions (*38*) indicates that the negatively charged species play a role in the self-assembly of misfolded proteins. It is obvious that the negatively charged phosphate diester backbones of DNA might play a role in the aggregation of SOD1. Finally, it has been reported that interactions between DNA and some proteins including cellular prion protein (PrP), α-synuclein, and human muscle acylphosphatase promote the formation of spherical amyloids and fibrils containing these proteins (*40*−*44*). The results obtained here show that DNA that acts as a template significantly accelerates the formation of SOD1 aggregates, confirmed by light scattering, size measurement, dye binding, imaging under visible and fluorescence light, and atomic force microscopy (AFM).

EXPERIMENTAL PROCEDURES

Materials. Bovine SOD1, calf thymus DNA (ctDNA), guanidinium chloride (GdmCl), ethidium bromide (EtBr), thioflavin S (ThS), and 8-anilino-1-naphthalene-sulfonic acid (ANS) were obtained from Sigma. GeneGreen (GG) is a gift from Tiangen. The plasmid pRK5 DNA, pBR322 DNA, bacteriophage λDNA, and double-stranded DNA fragment (dsDNA, 792 base pairs that are randomly distributed over DNA double strands) were obtained from TaKaRa. Removal of impurity from the SOD1 samples was monitored by LC−ESI-MS on an Agilent1100 Cap LC/MSD XCT mass spectrometer. The dimer concentration and activity at pH 5.5 of SOD1 was determined as previously reported (*45*, *46*). Unless otherwise stated, DNA concentrations were expressed in base pairs. All samples were prepared using distilled water that had been passed through a Millipore-Q ultrapurification system.

Quenching of SOD1 Intrinsic Fluorescence by DNA. To monitor quenching of SOD1 intrinsic fluorescence, 4.0 μM SOD1 was titrated with 0.8−30 μM ctDNA in 20 mM acetate (pH 3.6) at 37 °C. The tyrosine fluorescence of SOD1 was excited at 277 nm, and emission spectra were recorded between 290 and 350 nm (bandwidth 5 nm), or the emission intensity was recorded at 305 nm on a JASCO 770 spectrofluorometer. All reactions were incubated for 1 min at 37 °C to reach pre-equilibrium prior to measurements. The fluorescence of each DNA concentration was subtracted from the total intensity of the corresponding sample.

Aggregation of SOD1 upon Addition of DNA. Aggregation reactions consisted of SOD1 (0−15 μM) and any one of pRK5 DNA, λDNA, ctDNA, and dsDNA with varied concentrations, whereas control reactions were each concentration of SOD1 and each one of the DNAs, respectively. Reactions were initiated by adding DNA into SOD1, and were incubated for 0−2 h and 1, 2, and 15 days at 37 °C in 20 mM acetate buffer (pH 3.6), respectively, and then were quenched by cooling to 0 °C. In order to examine the effect of ionic strength on the aggregation of SOD1, a mixture of 4 μM SOD1 and 7.5 μM ctDNA was incubated for 2 h at 37 °C in the buffer containing 10−800 mM NaCl or $MgSO_4$. The pH effect was observed in a three-buffer system (20 mM phosphate-citric acid, pH 3.0−3.6; 20 mM HAc−NaAc, pH 3.6−5.6; and 20 mM Tris-HCl, pH 6.0−7.4). On the other hand, inhibition of the aggregation by the chemical

denaturant GdmCl was examined by incubating a mixture of 4 μM SOD1 and 7.5 μM ctDNA or 15 μM pBR322 DNA for 2 h at 37 °C in the acetate buffer containing 0−6.0 M GdmCl or 0−8 M urea. GdmCl was also used to promote the disaggregation of SOD1 aggregates. The disaggregation reactions occurred after adding 0−6.0 M GdmCl into SOD1 aggregates provided by 24 h of incubation.

Agarose Gel Electrophoresis. The mixtures containing SOD1 and DNA were electrophoresed on a 0.5× TBE buffer (45 mM Tris, 45 mM boron hydroxide, 1 mM EDTA, pH 8.0) agarose (0.8%) gel at 80 V. The DNA bands in the gel were visualized by staining in an EtBr solution (0.5 μg/mL) and quantified by a Bio-Rad phosphoimaging autodensitometer.

Right Angle Light Scattering (RALS) (17, 47). RALS measurements were made at 37 °C with the JASCO spectrofluorometer for each sample and each control (300 μL, including aggregation kinetic assays). Excitation and emission wavelengths were set at 400 nm (different bandwidths used here). All of the samples were vortexed in the buffer to dislodge aggregates prior to measurement. Each spectrum represents an average of ten accumulations.

Dynamic Light Scattering (DLS) (17, 26). At various time points, samples were analyzed by DLS to determine their extent of aggregation. DLS data were collected at 37 °C with a HORIBA LB-550 dynamic light scattering particle size analyzer. Consecutive measurements (200 times) were made with a cell of 2 mL. The average hydrodynamic diameters and their distribution were recorded for each sample and each control.

Single- and Double-Fluorescence Staining Imaging (18, 26, 40, 47). Fluorescence and visible microscopy studies of the dyes ThS and EtBr or GG, and both, bound to SOD1 aggregates were carried out via three pathways using the Olympus IX71 microscope under fluorescence (excitation wavelength 330−385 nm for ThS, 520−550 nm for EtBr, and 460−490 nm for GG) and visible light, respectively. All samples were preincubated for 10 min at 37 °C with 20 μM ThS, 20 μM EtBr or GG (1×) or their combinations in the acetate buffer (pH 3.6) before imaging. First, the aggregates provided by 1 or 15 days of equilibration at 37 °C of a mixture containing 4 μM SOD1 and 30 μM DNA were directly observed under the microscope without centrifugation. Then, the sample produced by 2 h of incubation of a mixture of SOD1 and DNA was examined via two pathways (*1*). The samples were sandwiched between two glass slides to obtain clear images of aggregates under the hydrated state (*2*). The aggregates were collected by centrifugation (8000 rpm, 10 min, 4 °C). The sediments were spread on a glass slide, washed, and air-dried, followed by examination under the Olympus microscope. All of these operations were carried out for SOD1 and DNA controls.

Visualization by AFM (27, 48). All images were obtained under dry conditions using a Seiko SPA400 atomic force microscope. The aggregates collected by centrifugation (8000 rpm, 10 min, 4 °C) were diluted with the buffer, deposited, washed, and air-dried onto freshly cleaved mica for measurement. Contact mode images were obtained using typical models.

Fluorescence Property of ANS Bound to SOD1 Aggregates (17, 40). The fluorescence property of the extrinsic fluorophore ANS (final concentration 20 μM, excitation at 360 nm, bandwidth 5 nm) was examined by 10 min of incubation at 37 °C with SOD1 alone or aggregates in the buffer (pH 3.6) on the JASCO 770 spectrofluorometer.

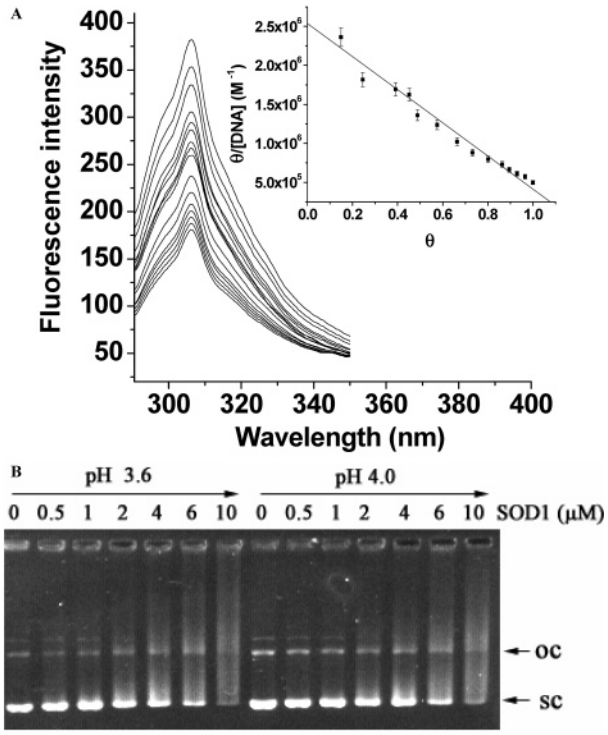

FIGURE 1: Affinity of SOD1 for DNA was examined by quenching of SOD1 intrinsic fluorescence and DNA gel shift assay. (A) 4.0 μM SOD1 was titrated with 0.8−30 μM ctDNA in 20 mM acetate buffer (pH 3.6). The control was 4.0 μM SOD1. Reactions were incubated for 1 min at 37 °C to reach pre-equilibrium prior to measurement. The inset is a Scatchard fitting to the plot of θ/[DNA] against θ to estimate the apparent dissociation constant of DNA−SOD1 complexes. Here, θ is the binding fraction of SOD1 to ctDNA. (B) The DNA retardation phenomenon in gel electrophoresis was shown after reactions containing 10 μM pBR322 DNA and 0−10 μM SOD1 were incubated for 60 min at 37 °C at pH 3.6 and 4.0.

RESULTS

Affinity of SOD1 for DNA. Quenching of SOD1 intrinsic fluorescence by DNA was used to characterize the interactions between SOD1 and DNA at pH 3.6. The fluorescence (290−350 nm) of tyrosine was specifically excited at 277 nm because bovine SOD1 does not contain any tryptophan residue. DNA produces no significant emission at this excitation wavelength in the region. The intrinsic fluorescence of SOD1 decreased as ctDNA concentration rose, whereas the emission of SOD1 control remained unchanged (Figure 1A), indicating that association of SOD1 with DNA may occur. Fitting the quenching curve (see the inset in Figure 1A) to a Scatchard equation (*49*) provides an apparent affinity constant of $K_d \sim 500$ nM, indicating that SOD1 can bind to DNA at pH 3.6. However, this fitting is very simple, since there are not available models for the binding events where protein aggregation may simultaneously appear. The observation that SOD1 can associate

with DNA was supported by DNA gel shift assays at pH 3.6 and 4.0 (Figure 1B). The results show a significant smear and mobility retardation phenomenon in the electrophoresis of plasmid DNA as SOD1 concentration rises, compared to DNA controls without SOD1, suggesting that the SOD1 binding to DNA is nonspecific to DNA sequences.

Formation of SOD1 Aggregates upon Addition of DNA. The determination of affinity above implies that DNA might induce a large number of SOD1 molecules to associate with it. Moreover, comparison with other proteins tested has indicated that the association with DNA is specific for some copper proteins including SOD1 (*29*, *50*). Because the aggregation of SOD1 upon addition of DNA is a phenomenon that we have noted during observation of the SOD1-mediated DNA cleavage activity (*29*, *50*), we examined the formation and morphology of aggregates resulting from incubation of the mixtures of SOD1 and DNA at pH 3.6 biophysical and biochemical methods. The used dyes EtBr and GG (*51*) are specific for DNA, whereas the dye ThS is highly specific for the cross-β-sheet structures in aggregates. Moreover, the ThS binding is accompanied by a large red shift in its excitation spectra. ThT was not used here because it interferes with the amyloid detection in the presence of DNA (*44*).

ThS-binding experiments were first used to characterize the formation of SOD1 aggregates upon addition of DNA. The presence of DNA alone cannot exert obvious influence on ThS fluorescence, but SOD1 alone can lead to an increase of ~17% in ThS fluorescence (Figure 2A), indicating that SOD1 undergoes an aggregation process at pH 3.6. A 1- or 2-fold enhancement of ThS fluorescence with 20−60 nm red shift in its excitation spectra (Figure 2B), relative to the reaction containing SOD1 alone, was observed with the mixtures of SOD1 and DNA (increasing concentration), suggesting that an aggregation phenomenon may appear between SOD1 and DNA, implying that the aggregates generated upon addition of DNA may have an ordered structure-like feature with cross-β-sheet structures (*52*). In addition, it was here noted that the enhancement in ThS fluorescence markedly depends on the sizes or types of DNA molecules tested (Figure 2B).

The fluorescence imaging of ThS is a method to characterize the morphology of protein aggregates. As controls, SOD1 and DNA all did not appear in any observable form of aggregates under microscope, indicating that the aggregation of SOD1 without DNA can be left out of consideration here. The ThS fluorescence images (Figure 3A) showed that the aggregates produced by incubating a mixture of SOD1 and λDNA were an amyloid-like and amorphous species. The same results hold for other DNA molecules tested (see Figure S1A,B).

In order to further examine the morphology of SOD1 aggregates, direct imaging of samples under the hydrated state was performed. First, the images of hydrated aggregate samples in solution stained by GG showed that the granular aggregates contain DNA (Figure 3B). Then, the bubbles that can collect a large number of aggregates were fixed between two glass slides. Clear images of GG-staining particles were observed under excitation light of 460−490 nm (Figure S1C,E,G). Finally, the particles were directly observed under visible light (Figure S1D,F,H). Obviously, these pictures are well consistent with each other. However, the

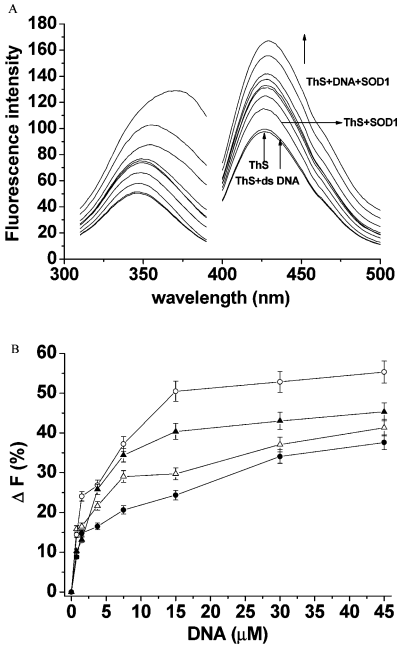

FIGURE 2: Comparison of ThS binding to SOD1, dsDNA, and SOD1 aggregates formed upon addition of ctDNA (○), λDNA (▲), pRK5 DNA (△), or dsDNA (●) in 20 mM acetate buffer (pH 3.6). Mixtures of 4 μM SOD1 with and without 0.75−45 μM DNA were incubated for 120 min at 37 °C. The resulting solutions were reincubated for 10 min at 37 °C with 20 μM ThS before measurements. (A) The excitation (left, emission wavelength 460 nm) and emission (right, excitement wavelength 340 nm) spectra of ThS bound to 4 μM SOD1, 45 μM dsDNA, or mixtures of SOD and dsDNA of increasing concentration. (B) DNA dependences of enhancement in emission intensity of ThS for the mixtures of SOD1 and DNA. Here, ΔF represents an enhancement percentage in the fluorescence of ThS caused by the mixtures of SOD1 and DNA relative to SOD alone, respectively.

fact that the particles under the dried state are larger and more amorphous in morphology (Figures 3A, and S1A,B), compared to the particles under the hydrated state, can be ascribed to a conglomeration of small aggregates. Here, it was noted that the dsDNA-containing particles have a narrow distribution of sizes (2−6 μm), whereas the distribution is very wide (2−20 μm) for ctDNA molecules with different sizes.

Double-fluorescence staining experiments were also performed with both ThS and EtBr to obtain a line of evidence for the composition of SOD1 aggregates. The results showed that the image with ThS staining is well superimposed over that with EtBr (Figures 3C,D, and S1I,J). These results, together with those delineated above, reveal that the aggregates contain both SOD1 and DNA, and the dye ThS is specifically bound to protein parts in the aggregates, and EtBr is specifically bound into DNA double helix.

For 15 days of incubation at 37 °C, a precipitate resulting from a mixture of SOD1 and ctDNA was directly observed without centrifugation. The precipitate was also stained with EtBr (Figure S1K) in addition to ThS (Figure 3E), and observed in hydrated states under the excitation light with variable wavelengths, indicating that the precipitate is a kind of macroaggregate. Obviously, the larger particles are formed by further self-assembly of a great body of small aggregates, since their diameters are at the micrometer level, and were not found in 2 h of incubation. The EtBr staining showed that the macroaggregates have morphological characteristic

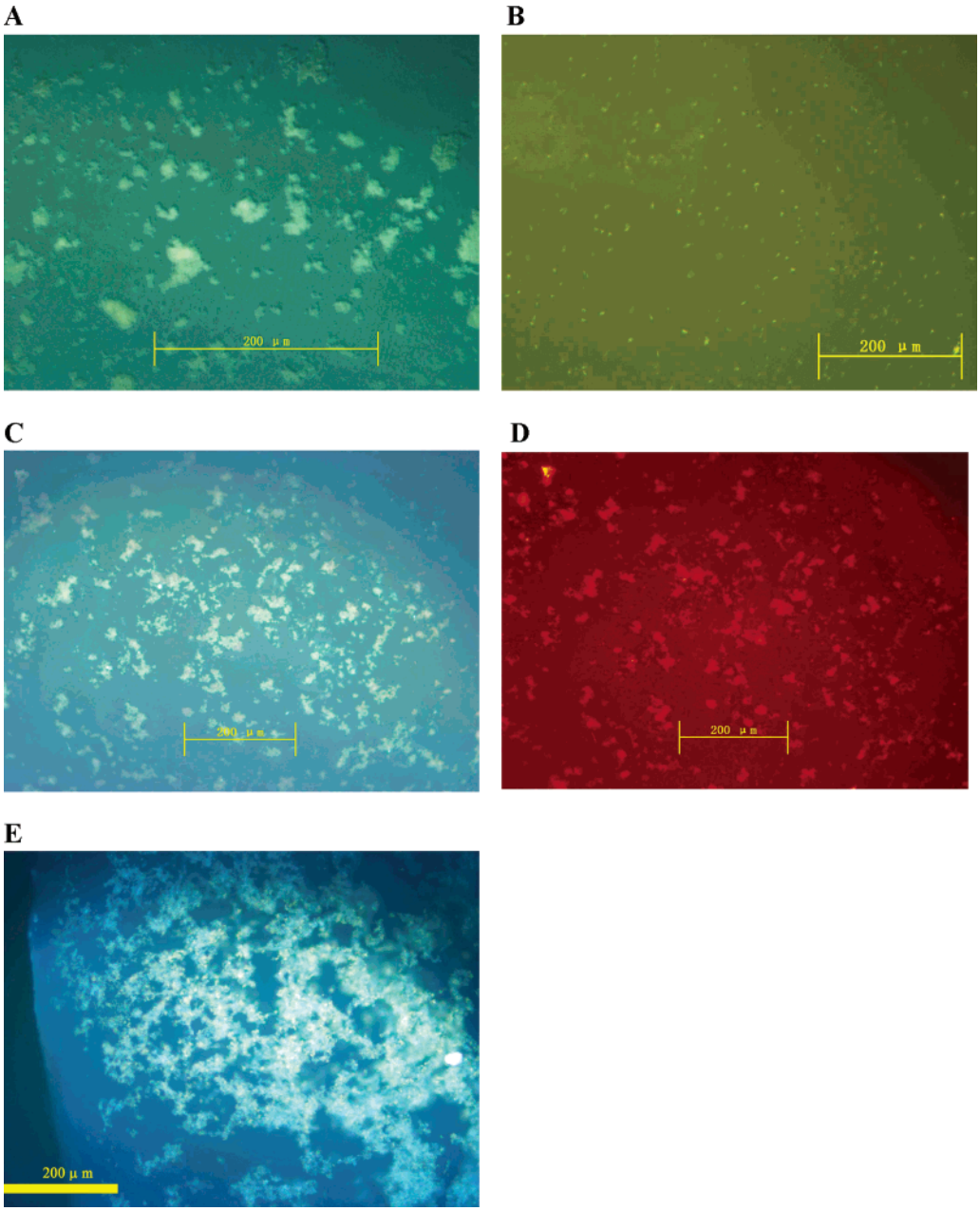

FIGURE 3: Visualization of SOD1 aggregates formed in the presence of DNA in 20 mM acetate buffer (pH 3.6) at 37 °C. The aggregates produced by 2 h of incubation were collected by centrifugation, followed by being suspended into the same volume of buffer prior to staining, and those done by 2 or 15 days of incubation were directly stained. Each dye was reacted for 10 min at 37 °C with various forms of SOD1 aggregates prior to imaging. (A) ThS (amplication 400×)-staining images of aggregates formed by incubating for 2 h a mixture of 4 μM SOD1 and 15 μM λDNA. (B) GG-staining image (200×) of hydrated aggregates produced by incubating for 2 days a mixture of 4 μM SOD1 and 7.5 μM λDNA. (C, D) Images (200×) of aggregates simultaneously stained with both ThS (C, excitation at 330−385 nm) and EtBr (D, excitation at 520−550 nm), after incubating for 2 h a mixture of 4 μM SOD1 and 37.5 μM dsDNA. (E) ThS-staining images (200×) of hydrated precipitates resulted from incubating for 15 days a mixture of 4 μM SOD1 and 30 μM ctDNA.

similar to that by ThS staining, a demonstration that the DNA are incorporated into the macroaggregates, as observed above.

AFM examination showed that granular particles with diameters of 200−1000 nm (Figure 4A) were formed by incubating the mixtures of SOD1 and DNA, a firm support to the observations done by the fluorescence imaging. For SOD1 as control, we did not observe a significant aggregation phenomenon. The AFM images indicated that the sizes of aggregates were markedly reduced with diluting the mixtures of SOD1 and DNA, suggesting that the larger particles are provided by self-assembly of small aggregates, as indicated by long periods of incubation. This was supported by the observation that the diameter distribution of aggregates was changed with time (see Figure 5A). The AFM images obtained by 10-fold dilution of the mixtures (Figure 4B−C) indicated that the aggregates absorbed to the mica surfaces are spherical and ellipsoidal. Their average diameter (~40 nm over 40 particles) and narrow diameter distribution were well consistent with those measured by DLS at the initial aggregation moment (<2 min, see Figure 5A). Therefore, the small particles were generated at the initial aggregation stage after SOD1 was bound to DNA.

Time Courses of SOD1 Aggregation. In conjunction with visualization studies, time-course analysis of SOD1 aggrega-

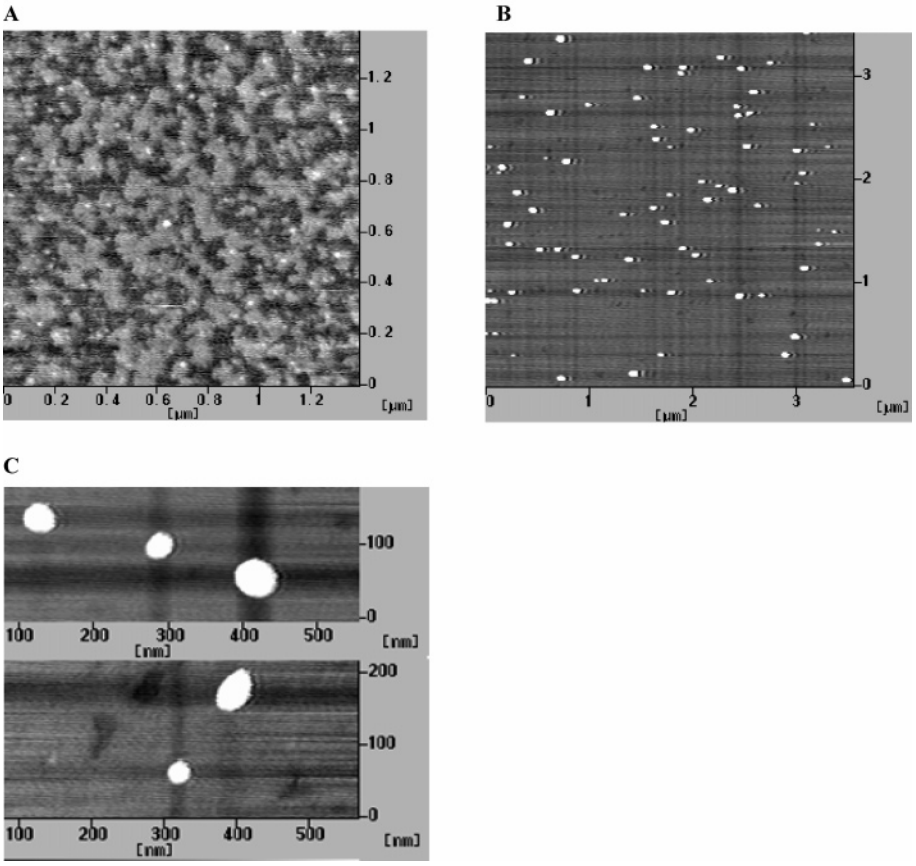

FIGURE 4: AFM images of aggregates formed by incubating for 2 h a mixture of SOD1 and DNA in 20 mM acetate buffer (pH 3.6) at 37 °C. The aggregates collected by centrifugation, followed by being suspended into the same volume of buffer, were deposited and air-dried onto freshly cleaved mica. (A) AFM image of aggregates formed by incubating a mixture of 4 μM SOD1 and 50 μM dsDNA. (B, C) The solution containing the aggregates was diluted by 10-fold with the buffer and immediately added to the mica surface for AFM.

tion upon addition of DNA was performed using DLS and RALS to quantify the sizes of aggregates in terms of average hydrodynamic diameters. The experiments were carried out in the presence and absence of DNA, respectively, to assess the promotion effect of DNA as a template on the SOD1 aggregation. The sizes of SOD1 dimer (~6.6 nm × 4.1 nm × 3.7 nm) (*26*) and DNA exhibit no observable change before and after incubation. However, it is difficult to obtain the real sizes of SOD1 and DNA of interest, due to the limited precision of the instrument used.

The DLS data showed that upon addition of DNA an aggregation phenomenon was immediately observed, indicating that DNA is an accelerating agent for SOD1 aggregation because SOD1 has relatively low propensities to aggregate in solution. The aggregation processes of SOD1 pass through two phases (Figure 5A). The reactions first undergo a rapid phase where the aggregates with average diameters of 40−80 nm (dependent on the type of DNA) rapidly form in <2 min, and then pass through a slow phase where the average diameters of aggregates were increased nearly linearly to 200−260 nm over time (Figure 5A,B). Here, it is not possible to measure the sizes of aggregates in the rapid phase because the shortest data-collecting time required by the DLS is 2 min. After 2 h of incubation, the sizes of aggregates yet remained at a slight increase. The time courses of aggregation monitored by RALS, in good agreement with those by DLS, showed a kinetic process (Figure 5C) in that the sizes of aggregates were sharply increased at the initial time point of reaction. In contrast, for ctDNA or dsDNA as control, no change in RALS data over time is observed under the conditions tested. For SOD1, an increase of ~10% in RALS data is due to its self-aggregation at pH 3.6, in agreement with those reported previously (*26*). In addition, it was here also noted that the initial rates of aggregation were different for different DNA molecules (see the inset in Figure 5C).

Effects of Solution Conditions. The effects of solution conditions including types of DNA, SOD1 concentration, pH, ionic strength, and chemical denaturant GdmCl on the aggregation of SOD1 were examined. The imaging analysis and time courses delineated above have shown that the SOD1 aggregation was significantly affected by types of DNAs tested. Therefore, four types of DNAs were tested at pH 3.6 by DLS and RALS. First, it was observed that the sizes of aggregates increase in the order ctDNA > pRK5 DNA ≈ λDNA > dsDNA in the range of given DNA levels (<50 μM) (Figure 6A,B), indicating (a) that the sizes of DNA molecules are one of the factors that control the aggregation and (b) that the large and linear ctDNA and λDNA molecules led to the formation of large aggregates. This fact might be ascribed to different length and structures of the DNAs. The plasmid DNA has a compactly supercoiled structure, leading to the sizes of aggregates that are close to those of aggregates by λDNA, although its base pairs (~8000) are much less than those of λDNA (~48000 base pairs). The small and linear dsDNA molecules can provide only a limited space for the aggregation of SOD1, leading to the formation of the smaller aggregates.

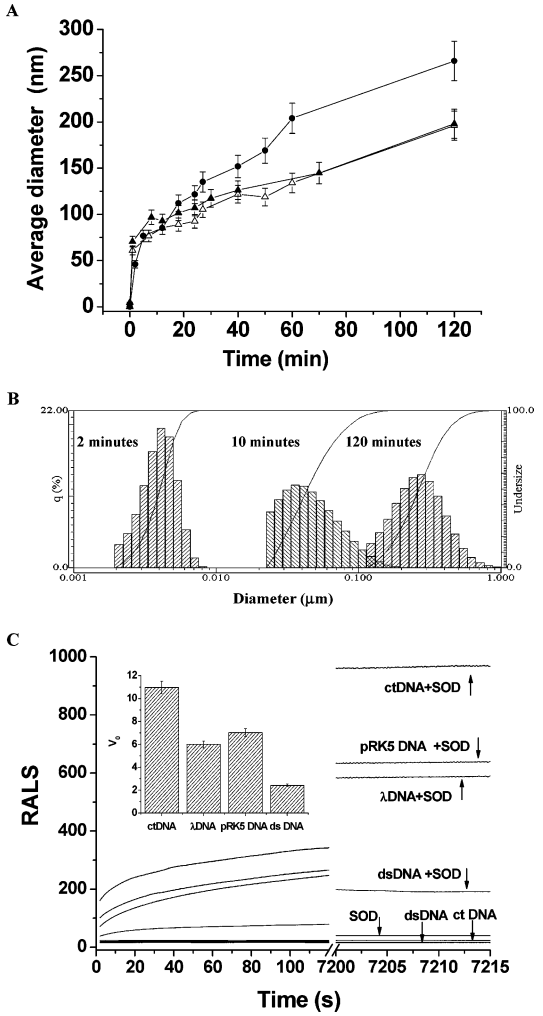

FIGURE 5: The time courses of SOD1 aggregation upon addition of DNA in 20 mM acetate buffer (pH 3.6) at 37 °C were observed by DSL and RALS. (A) The average diameters of aggregates generated from reactions containing 4 μM SOD1 and 7.5 μM pRK5 DNA (△), λDNA (▲), or 37.5 μM dsDNA (●) were changed with time (0−120 min). (B) The diameter distributions of aggregates between SOD1 and pRK5 DNA were measured by DSL at different time points. (C) The aggregation processes of SOD1 in the presence of 7.5 μM pRK5 DNA, λDNA, ctDNA, or dsDNA were monitored by RALS. The inset shows that the initial rates of aggregation were changed with types of DNA. The control was the corresponding concentration of SOD or DNA alone.

The effect of SOD1 concentration on the sizes of aggregates was observed by fixing ctDNA concentration (7.5 μM). The RALS data show that, first, the sizes were sharply, but linearly, increased when SOD1 concentration was
$<$0.5 μM, then remained at a slight increase when SOD1 was $>$5 μM (Figure 6C), indicating that DNA can promote nanomolar levels of SOD1 to aggregate. Increasing SOD1 concentration only led to a weak enhancement (by 1.5-fold up to 16 μM SOD1) in fluorescence of ThS bound to the aggregates, suggesting that the aggregates do not possess fibrous characteristics because fibrous aggregates can lead to a 3-fold enhancement in ThS fluorescence (*40*).

The pH dependences of aggregation of SOD1 upon addition of DNA were observed by RALS and gel electrophoresis. The RALS data show (a) that the formation of SOD1 aggregates after 2 h of incubation with DNA was significant and their sizes remain basically unchanged at pH $<$ 4.0, and (b) that an observable aggregation phenomenon was not found at pH $\geq$ 4.5 (Figure 6D), in agreement with the smearing phenomenon observed by the gel retardation experiments (Figure 6E), demonstrating that the aggregation of SOD1 does not occur even in the presence of DNA when the pH is more than 4.5.

Probing the effect of ionic strength on the aggregation can provide an insight into the nature of interactions between SOD1 and DNA. First, we observed that quenching of SOD1 intrinsic fluorescence by DNA was markedly reduced with increasing Na^+ or Mg^{2+} concentration, indicating the interactions between both become progressively weaker. Then, RALS data showed that the high ionic strength markedly inhibited the aggregation (at 800 mM Na^+ or Mg^{2+}, reduction of 87% or 89% in aggregation degree, Figure 6F). All these data suggest that electrostatic interactions are one of the key factors that control the enrichment of SOD1 along DNA double strands.

In addition, a significant inhibition of the aggregation was observed at pH 3.6 upon addition of chemical denaturant GdmCl or urea. First, the inhibition was examined by RALS, indicating that 2 M GdmCl or urea led to a reduction of 90% or 80% in aggregation degree (Figure 6G, Figure S2). Then, the disaggregation experiments (Figure 6H) showed that the disaggregation of SOD1 aggregates takes place immediately upon addition of GdmCl, supported by DNA electrophoresis experiments (Figure S3). For example, 2 and 6 M GdmCl led to disaggregation of 77% and 90% of aggregates in 1 min, respectively. The data indicate (a) that the SOD1 intermolecular hydrophobic interactions play a crucial role in the DNA-accelerated SOD1 aggregation because urea can disrupt these hydrophobic interactions, and (b) that the electrostatic forces between SOD1 and DNA play only a role of concentrating SOD1 molecules along DNA double strands because the guanidinium cations at a high level (6 M) can disrupt this force by competing against SOD1 in binding to DNA. It is noteworthy in Figure S3 that the DNA molecules released from the aggregates remained intact, revealing that the DNA was not damaged in the aggregation.

Changes in Hydrophobicity. The hallmark of SOD1 is exceptional stability and specificity of fold due to conserved features within the Greek-key β-barrel structure (*1*). However, due to lower pH coupled with the presence of DNA, the SOD1 hydrophobicity might be altered to a certain degree. Therefore, in order to determine if changes in hydrophobicity occur, ANS dye binding experiments were first performed before and after SOD1 binding to DNA. ANS binding is a probe of exposed hydrophobic surfaces in proteins that indicates the disruption and formation of hydrophobic clusters. The wild-type SOD1 does not show any ANS binding. However, the ANS fluorescence was observed to have a 2-fold enhancement for the SOD1 alone after 2 h of incubation, likely due to a conformational change resulting from removal of metals at low pH (*27*). On the other hand, DNA of different forms was also observed to enhance considerably the ANS fluorescence under conditions tested. Figure 7A shows the influence of DNA on ANS fluorescence bound to SOD1 aggregates. Here, the total enhancement value in the ANS fluorescence caused by the respective presence of DNA and SOD1 was subtracted from those caused by SOD1 aggregates upon addition of DNA at

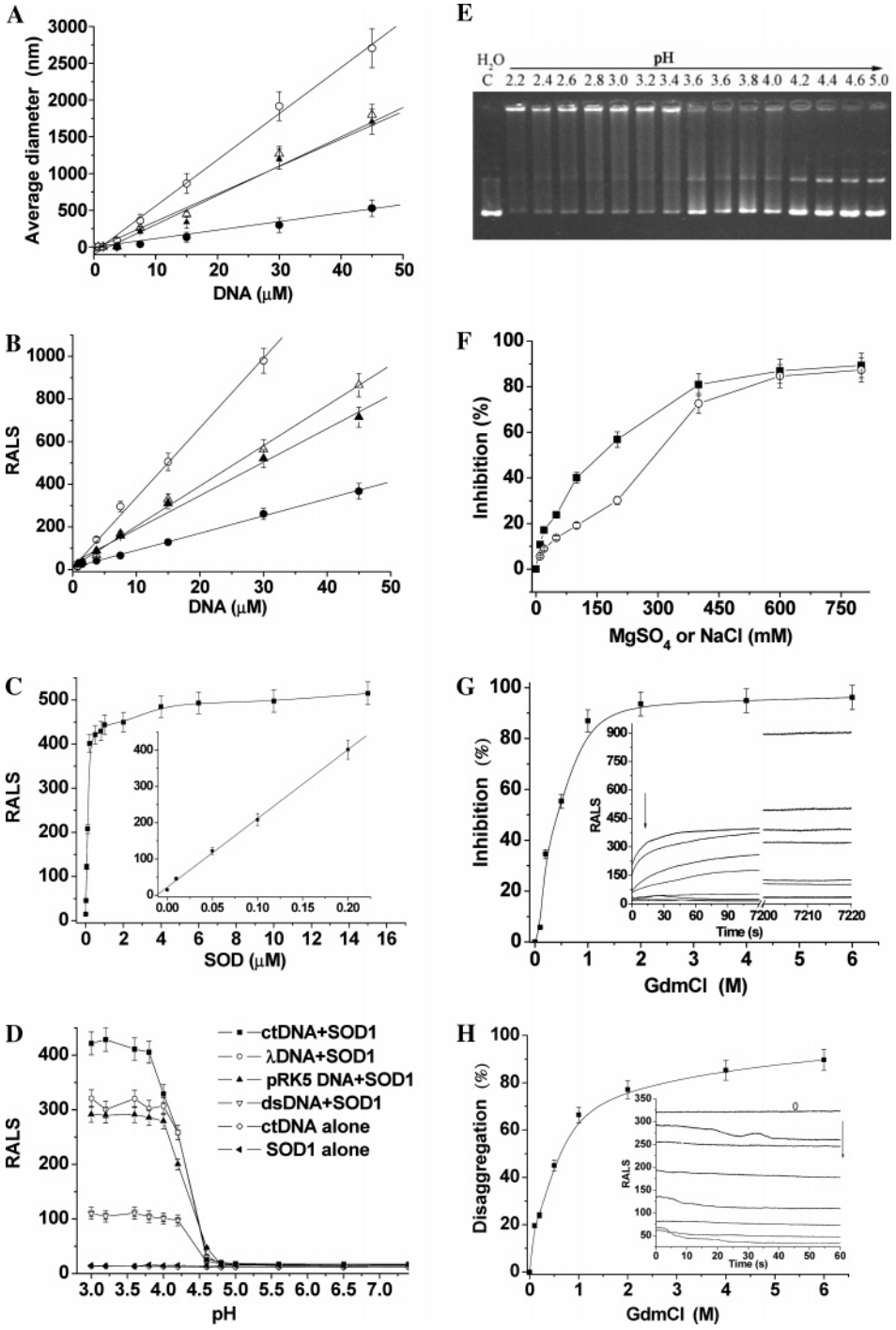

FIGURE 6: The dependences of SOD1 aggregation at 37 °C on reaction conditions. (A, B) The dependences of SOD1 aggregate sizes on types and concentrations of DNA were monitored by DSL (A) and RALS (B). Reactions containing 4 μM SOD1 and 0.75−45 μM ctDNA (○), pRK5 DNA (△), λDNA (▲) or dsDNA (●) were incubated for 2 h in 20 mM acetate buffer (pH 3.6) prior to measurements. (C) The dependence of SOD1 aggregation on its concentration was monitored by RALS. Reactions containing 0−16 μM SOD1 and 7.5 μM ctDNA were incubated for 2 h. (D, E) The pH dependences of of DNA-accelerated SOD1 aggregation were observed by RALS (D) and gel electrophoresis (E). A three-buffer system (pH 3.0−3.6, 20 mM phosphate-citrate; pH 3.6−5.6, 20 mM HAc−NaAc, and pH 6.0−7.4, 20 mM Tris-HCl) was used for measurements between pH 3.0 and 7.4. Reactions containing 4 μM SOD1 and 7.5 μM ctDNA, pRK5 DNA, λDNA, dsDNA (D), or 4 μM SOD1 and 15 μM pBR 322 DNA (E) were incubated for 2 h prior to measurements. The controls were corresponding type of DNA or SOD. (F) The effect of ionic strength on SOD1 aggregation was monitored by RALS. Reactions containing 4 μM SOD1 and 7.5 μM ctDNA were incubated for 2 h in the buffer containing 0−800 mM NaCl (○) or $MgSO_4$ (■). (G, H) Inhibition of aggregation and disaggregation of aggregates caused by GdmCl were monitored by RALS. Inhibition reactions contained 4 μM SOD1 and 7.5 μM ctDNA in the buffer containing 0−6 M GdmCl (G). Disaggregation reactions contained 0−6 M GdmCl and aggregates formed by incubating for 24 h a mixture of 4 μM SOD1 and 7.5 μM ctDNA (H). The insets are time courses of inhibition or disaggregation reactions.

each concentration. The data showed that the ANS fluorescence was nearly increased by up to 4−9-fold, accompanied by a large blue shift in the ANS fluorescence maximum from 532 to 473 nm, with DNA concentrations. Obviously, this large enhancement is caused by SOD1 aggregates, but not by the simultaneous presence of DNA and SOD1, because

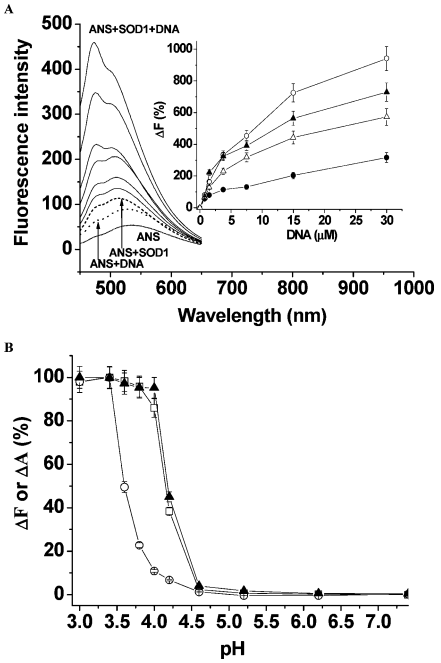

FIGURE 7: Changes in hydrophobicity of SOD1 measured by ANS binding and intrinsic fluorescence quenching of SOD1. (A) Fluorescence spectra of ANS bound to the aggregates formed by incubating for 2 h 4 μM SOD1, 30 μM dsDNA, or the mixtures of SOD and 0−30 μM dsDNA at 37 °C. The inset shows that DNA concentration dependences of enhancements in the fluorescence of ANS bound to the aggregates formed by incubating mixtures of 4 μM SOD1 and 0−30 μM ctDNA (○), pRK5 DNA (△), λDNA (▲), or dsDNA (●). Here, ΔF represents an enhancement percentage in the ANS fluorescence intensity at 473 nm caused by the aggregates relative to ANS alone. The enhancement values in the ANS fluorescence caused by DNA alone and SOD alone were subtracted from those caused by the aggregates at each DNA concentration, respectively. (B) The pH-dependent profiles of changes in both the fluorescence intensity of ANS bound to the aggregates and the intrinsic fluorescence intensity of SOD1 alone. The 4 μM SOD1 alone or mixtures of 4 μM SOD1 and 20 μM ANS were incubated for 2 min in pH 3.0−3.6, 20 mM phosphate-citrate; pH 3.6−5.6, 20 mM acetate; and pH 6.0−7.4, 20 mM Tris-HCl, respectively, prior to measurements. Here, ΔF (△) represents a normalized reduction in the intrinsic fluorescence intensity of SOD1 at 305 nm at each pH tested relative to SOD1 at pH 7.4. ΔF (○) represents a normalized enhancement in ANS fluorescence intensity at 520 nm caused by the SOD1 relative to ANS alone at each pH tested. The pH-dependent data of aggregation degree was also normalized to correlate the aggregation degree with changes in hydrophobicity. Here, ΔA (▲) was used to represent a normalized enhancement in aggregation degree of SOD1 upon addition of ctDNA in Figure 6D relative to SOD1 alone.

low pH coupled to the interactions with DNA can cause conformational changes in SOD1, resulting in exposure of more hydrophobic residues to the surfaces. In addition, the ANS fluorescence enhancement shows that types of DNA molecules tested can obviously affect exposure degrees of SOD1 hydrophobic residues. The large DNA molecules such as ctDNA and λDNA lead to a larger fluorescent enhancement (see the inset in Figure 7A), causing more SOD1 molecules to alter their conformation than does the small DNA.

Then, the pH-dependent profiles of ANS binding and intrinsic fluorescence quenching of SOD1 were examined and the data were normalized for comparison (Figure 7B). Moreover, the pH dependence of aggregation degree measured by RALS was also normalized to correlate the aggregation degree with the changes in hydrophobicity. The results indicate that the ANS fluorescence was enhanced and the intrinsic fluorescence was quenched with lowering pH, revealing that the low pH resulted in exposure of more hydrophobic residues to the surface of SOD1 and an enhanced propensity of SOD1 to form aggregates. This was firmly supported by the fact that the pH-dependent curve of intrinsic fluorescence quenching of SOD1 was well superimposed over that of aggregation degree and was well consistent with pH dependences of DNA-accelerated SOD1 aggregation at a given DNA level (Figure 6D).

DISCUSSION

The aim of this study was to identify the potential target of SOD1 aggregation-induced cytotoxicity and to contribute to our understanding to the previous reports by illustrating that the interaction with DNA may affect the aggregation pathways of SOD1. The results presented indicate that the aggregation of SOD1 upon addition of DNA occurs rapidly under the conditions tested. The resulting DNA-containing SOD1 aggregates are unlikely to be nonspecific staining artifacts because they were directly observed under both hydrated and dried states by single- and double-fluorescence labeling microscopy, light scattering, and AFM imaging, and are similar to those observed by previously reported studies in morphology (*16*, *19*, *25*). It is noteworthy that the double-labeling method used here, specific for both protein aggregates and DNA, respectively, is convenient and simple to characterize the complex compositions of DNA-containing protein aggregates.

Using the low pH conditions, which could mimic the effect of mutations and reflect the practical process done under physiological conditions to a high extent, is common to study the aggregation of SOD1 and other proteins (*26*, *27*). The acidic conditions have been shown to decrease the affinity of SOD1 for metals by protonation of the ligating histidine residues and to promote dissociation of SOD1 into monomers, resulting in loss of metals from SOD1 like MBR mutants (*53*, *54*). In fact, to create amyloidogenic conditions under which the aggregation of proteins can be induced readily, acidic conditions are routinely used. For example, amyloidogenic intermediates of transthyretin, microglobulin, prion protein, and lysozyme have been characterized at pH 4.5 (*55*), pH 3.6 (*56*), pH 4.4−6 (*57*), and pH 2 (*58*).

Interactions between SOD1 and DNA. The calculation of electrostatic potential has revealed some striking positively charged regions over SOD1 surfaces under neutral conditions (*59*), suggesting that SOD1 may be a potential DNA-binding enzyme, and the presence of positively charged residue side chain containing peptide segments could meet the requirement for DNA binding. The nonspecifically electrostatic interaction may occur between the positively charged residues over SOD1 surfaces and the negatively charged DNA backbone, supported by two facts. (a) The aggregation of SOD1 along DNA double strands was significantly inhibited with increasing ionic strength. (b) The affinity of SOD1 for DNA is pH-dependent because the dissociation constant of the enzyme−DNA complex is decreased from 10 μM at pH 7.4 (*29*) to 500 nM at pH 3.6, and low pH can result in an increase in the net positive charge on SOD1, strengthening the binding of SOD1 to DNA.

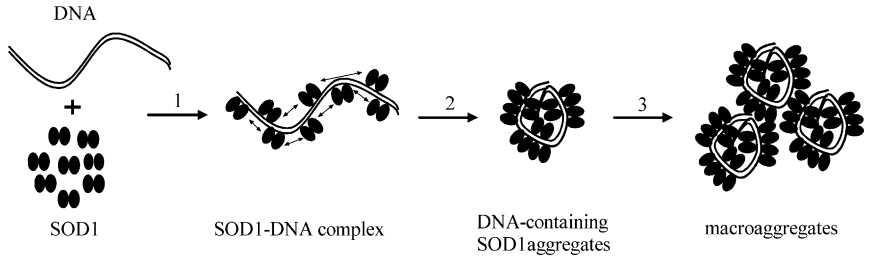

FIGURE 8: A proposed model of SOD1 aggregation upon addition of DNA.

Changes in Hydrophobic Interactions. Rapid aggregation, including formation of fibrous species, is often associated with the disruption of the native structure of a protein, provided that the latter is achieved under conditions whereby strong intermolecular interactions can occur (*60*). Such conditions can also include low pH and interactions with other species. Both low pH and interactions with DNA can result in a significant alteration in the native hydrophobic interactions and may permit a gain of non-native interactions among SOD1 subunits, supported by several lines of evidence. First, the enhancement in the ANS fluorescence upon addition of DNA reveals the formation and disruption of hydrophobic clusters (Figure 7A). Then, the pH-dependent change of SOD1 hydrophobicity was well consistent with pH dependences of DNA-accelerated SOD1 aggregation (Figure 7B), and SOD1 aggregates were degraded with given levels of either GdmCl or urea, indicating that SOD1 intermolecular hydrophobic interactions were predominantly responsible for the aggregation of SOD1. Finally, quenching of SOD1 intrinsic fluorescence (Figure 1) showed that at least the hydrophobic environments around the tyrosine residues are altered under the conditions tested. The low pH coupled to the binding to DNA not only affects the stability of SOD1, but also acts upon the free energy barrier to unfolding and aggregation.

Acceleration Role of DNA as a Template in SOD1 Aggregation. Protein aggregation has been shown to be affected by several factors, including protein concentration, interactions with other species, and macromolecular crowding. Under physiological conditions, almost any protein can be induced at high concentration to form amorphous aggregates (*60*). Obviously, the enrichment in SOD1 along DNA double strands is in agreement with this situation because the DNA-mediated SOD1 enrichment may mimic the in vivo macromolecular crowding environments. It has been reported that the interactions with the negatively charged fatty acids, micelle, heparin, or acidic peptides stimulate the in vitro polymerization of SOD1 (*38*), Aβ (*61*), tau (*62*), or α-synuclein (*28*). Nucleic acids have been observed to promote the formation of amyloid fibril and fibers of different morphologies by interacting with PrP, α-synuclein, human muscle acylphosphatase, and tau protein in solutions (*40*−*42*, *63*). The studies mean that the negatively charged species that may act as a template to promote further growth of aggregates play a pivotal role in self-assembly of misfolded proteins, and the resulting aggregation processes may be independent of protein amino acid sequences. Here, we observed that SOD1 was robustly converted into a small particle at the initial addition time point of DNA, and then a large particle was formed from the resulting small particles (Figure 5), indicating that the DNA-accelerated SOD1 aggregation is not in agreement with the situation of nucleation-dependent aggregation (*63*, *64*), although the possibility that the lag stage in the nucleation-dependent aggregation is minimized or removed by addition of DNA cannot be excluded.

A detailed time-course analysis of aggregation (Figure 5) was performed using light scattering experiments to quantify the sizes of aggregates in terms of their diameters. The same experiments were also carried out in the absence of DNA to assess the accelerating effect of DNA on the SOD1 aggregation. The data show that SOD1 was aggregated much more rapidly with DNA than without DNA, and than aggregation of SOD1 mutants (without DNA) (*16*, *26*). The aggregate particles of 40−80 nm were formed in <2 min of incubation upon addition of DNA, whereas the formation of SOD1 aggregates with such a diameter requires, in general, a growth period of many days or weeks in the absence of DNA (*27*). Thus, DNA acts only as a kinetic template that alters the aggregation pathways of SOD1 because the aggregation reactions are favorable in thermodynamics due to changes in hydrophobicity of SOD1.

Possible Pathways of SOD1 Aggregation. SOD1 is here shown to form large granular aggregates upon addition of DNA at SOD1 levels near to, or even less than, those found in the cytoplasm of neurons. Morphological comparison with those obtained previously in vivo and in vitro shows that the granular morphology of the DNA-containing SOD1 aggregates resembles those in both familial and sporadic forms of ALS, and in AD brains (*18*, *19*, *22*, *36*−*38*). The formation propensity of SOD1 aggregates correlates not only with electrostatic interactions between SOD1 and DNA but also with changes in the hydrophobicity of SOD1.

Although the precise mechanism of how the negatively charged molecule accelerates the formation of protein aggregates remains elusive, the DNA-accelerated SOD1 aggregation has some characteristics that are consistent with the proposed gain-of-interaction models (*31*, *65*). The conformational change of SOD1 exposes some previously inaccessible surfaces upon addition of DNA at low pH. These newly exposed surfaces bind to the corresponding surfaces of another SOD1 molecule, building up an aggregate. Therefore, a model is proposed to explain the possible pathways of SOD1 aggregation. As shown in Figure 8, first, it is clear that an orientation-specific binding of SOD1 to DNA double strands occur via the electrostatic interactions, leading to the neutralization of the positive charges of the SOD1 side chains that prevent from aggregation. The resulting removal of the positive charges could promote the association of SOD1 molecules with each other through the hydrophobic interactions. Then, the SOD1 molecules can assemble into aggregates along DNA double strands via a SOD1 proximity-dependent process that can be described as a one-dimension assembly like beads on a string, forming

a helical structure along DNA duplex. A DNA-filled nanotube might be produced via this pathway, in which the wall of nanotubes is consisted of SOD1 molecules. The nanotubes can further self-coil into a granular structure that may be spherical or ellipsoidal because they seem to be characterized by a high degree of flexibility. Finally, the granular aggregates can self-cluster into a macroaggregate. An alternative pathway may be that short and linear SOD1 oligomers associate with DNA via the electrostatic interactions, resulting in the direct formation of large particles. Addition of SOD1 into DNA-containing solutions might lead to appearance of the former pathway, and vice versa the latter pathway might be crucial.

In conclusion, the observations presented here establish that the rapid initiation of granular SOD1 aggregates is dependent on the presence of DNA, supporting the concept that DNA acts as a kinetic template that alters the aggregation pathways of SOD1 because the aggregation reactions are a favorable process in thermodynamics due to changes in hydrophobicity of SOD1 under acidic conditions. Although it is not known if nucleic acids are involved in the formation of SOD1 aggregates in vivo (*6*, *7*), nucleic acids have been detected in neurofibrillary tangles, intracellular inclusions primarily composed of the tau protein, as well as in senile plaques composed of Aβ (*39*).

Based on recently reported results (*38*−*44*, *60*−*63*), the negatively charged species-accelerated protein aggregation appears to be a general phenomenon and is likely to contribute significantly to the formation of proteinaceous aggregates and inclusions in vivo. Moreover, in light of the discussion above, the presence of nucleic acids might be expected to increase dramatically the strength of intermolecular hydrophobic interactions of proteins. Such an effect could have major consequences for a range of cellular functions. First, aberrant changes in hydrophobicity have directly or indirectly been observed for the fALS-related SOD1 mutants (*66*), and environmental conditions such as low pH and oxidation of metal-binding sites compromise the metal-binding ability of SOD1, as do MBR mutants (*2*−*5*, *26*−*28*, *53*−*54*), resulting in changes in hydrophobicity of SOD1 (*17*, *47*). Therefore, SOD1 of any one form with aberrant changes in hydrophobicity, even at very low levels, may form aggregates due to the enrichment effect of DNA in physiological pH conditions. Then, most notably, because DNA is the source of genetic information and a potential target of misfolded SOD1-induced cytotoxicity, the aggregation with DNA could have profound effects on viability and genetic stability, likely leading to destruction of DNA expression. Finally, an interesting implication in this work is that the formation of DNA-accelerated proteinaceous deposts might promote depletion of essential proteins. However, if the DNA-accelerated aggregation of SOD1 in solution can be borne out by further in vivo tests, there are significant therapeutic implications. Since there is recent evidence that the inclusions may be protective (*67*, *68*) and that earlier aggregation oligomers may be more toxic than larger inclusions (*67*−*70*), the formation of DNA-accelerated SOD1 inclusions would be become a potential pathway to avoid the accumulation of toxic protein oligomers.

SUPPORTING INFORMATION AVAILABLE

The dye-staining images of SOD1 aggregates formed upon addition of DNA (Figure S1) under visible and fluorescent light, and inhibition of aggregation caused by urea (Figure S2), and disaggregation of aggregates and inhibition of aggregation caused by GdmCl monitored by agarose gel electrophoresis (Figure S3). This material is available free of charge via the Internet at http://pubs.acs.org.

REFERENCES

1. Fridovich, I. (1975) Superoxide dismutases, *Annu. Rev. Biochem. 44*, 147−159.
2. Valentine, J. S., and Hart. P. J. (2003) Bioinorganic Chemistry Special Feature: Misfolded CuZnSOD and amyotrophic lateral sclerosis, *Proc. Natl. Acad. Sci. U.S.A. 100*, 3617−3622.
3. Hayward, L. J., Rodriguez, J. A., Kim, J. W., Tiwari, A., Goto, J. J., Cabelli, D. E., Valentine, J. S., and Brown, R. H., Jr. (2002) Decreased metallation and activity in subsets of mutant superoxide dismutases associated with familial amyotrophic lateral sclerosis, *J. Biol. Chem. 277*, 15923−15931.
4. Rodriguez, J. A., Valentine, J. S., Eggers, D. K., Roe, J. A., Tiwari, A., Robert H. B., Jr. and Hayward. L. J. (2002) familial amyotrophic lateral sclerosis-associated mutations decrease the thermal stability of distinctly metallated species of human copper/zinc superoxide dismutase, *J. Biol. Chem. 277*, 15932−15937.
5. Tiwari, A., and Hayward, L. J. (2003) Familial amyotrophic lateral sclerosis mutants of copper/zinc superoxide dismutase are susceptible to disulfide reduction, *J. Biol. Chem. 278*, 5984−5992.
6. Valentine, J. S., Doucette, P. A., and Potter, S. Z. (2005) Copper-zinc superoxide dismutase and amyotrophic lateral sclerosis, *Annu. Rev. Biochem. 74*, 563−593.
7. Bruijn, L. I., Miller, T. M., and Cleveland, D. W. (2004) Unraveling the mechanisms involved in motor neuron degeneration in ALS, *Annu. Rev. Neurosci. 27*, 723−749.
8. Cleveland, D. W., and Rothstein, J. D. (2001) From Charcot to Lou Gehrig: deciphering selective motor neuron death in ALS, *Nat. Rev. Neurosci. 2*, 806−819.
9. Deng, H. X., Hentati, A., Tainer, J. A., Iqbal, Z., Cayabyab, A., Huang, W. Y., Getzoff, E. D., Hu, P., Herzfeldt, B., Roos, R. P., Warner, C., Deng, G., Soriano, E., Smyth, C., Parge, H. E., Ahmed, A., Roses, A. D., Hallewell, R. A., Pericak-Vance, M. A., and Siddique, T. (1993) Amyotrophic lateral sclerosis and structural defects in Cu,Zn superoxide dismutase, *Science 261*, 1047−1051.
10. Rosen, D. R., Siddique, T., Patterson, D., Figlewicz, D. A., Sapp, P., Hentati, A., Donaldson, D., Goto, J., O'Regan, J. P., Deng, H. X., Rahmani, Z., Krizus, A., McKenna-Yasek, D., Cayabyab, A., Gaston, S. M., Berger, R., Tazni, R. E., Halperin, J. J., Herzfeldt, B., van der Bergh, R., Huang, W. Y. T., Bird, Deng, G., Mulder, D. W., Smyth, C., Laing, N. G., Soriano, E., Pericak-Vance, M. A., Haines, J., Roulean, G. A., Gusella, J. S., Harvitz, H. R., and Brown, R. H., Jr. (1993) Mutations in Cu/Zn superoxide dismutase gene are associated with familial amyotrophic lateral sclerosis, *Nature 362*, 59−62.
11. Gurney, M. E., Pu, H., Chiu, A. Y., Dal Canto, M. C., Polchow, C. Y., Alexander, D. D., Caliendo, J., Hentati, A., Kwon, Y. W., and Deng, H. X. (1994) Motor neuron degeneration in mice that express a human Cu,Zn superoxide dismutase mutation, *Science 264*, 1772−1775.
12. Hart, P. J. (2006) Pathogenic superoxide dismutase structure, folding, aggregation and turnover, *Curr. Opin. Chem. Biol. 10*, 131−138.
13. Boillee, S., Velde, C. V., and Cleveland, D. W. (2006) ALS: a disease of motor neurons and their nonneuronal neighbors, *Neuron 52*, 39−59.
14. Rodriguez, J. A., Shaw, B. F., Durazo, A., Sohn, H., Doucette, P. A., Nersissian, A. M., Faull, K. F., Eggers, D. K., Tiwari, A., Hayward, L. J., and Valentine, J. S. (2005) Destabilization of apoprotein is insufficient to explain Cu,Zn-superoxide dismutase-linked ALS pathogenesis, *Proc. Natl. Acad. Sci. U.S.A. 102*, 10516−10521.
15. Lindberg, M. J., Tibell, L., and Oliveberg, M. (2002) Common denominator of Cu/Zn superoxide dismutase mutants associated with amyotrophic lateral sclerosis: decreased stability of the apo state, *Proc. Natl. Acad. Sci. U.S.A. 99*, 16607−16612.

16. Stathopulos, P. B., Rumfeldt, J. A. O., Scholz, G. A., Irani, R. A., Frey, H. E., Hallewell, R. A., Lepock, J. R., and Meiering, E. M. (2003) Cu/Zn superoxide dismutase mutants associated with amyotrophic lateral sclerosis show enhanced formation of aggregates in vitro, *Proc. Natl. Acad. Sci. U.S.A. 100*, 7021−7026.
17. Rakhit, R., Crow, J. P., Lepock, J. R., Kondejewski, L. H., Cashman, N. R., and Chakrabartty, A. (2004) Monomeric Cu,-Zn-superoxide dismutase is a common misfolding intermediate in the oxidation models of sporadic and familial amyotrophic lateral sclerosis, *J. Biol. Chem. 279*, 15499−15504.
18. Choi, J., Rees, H. D., Weintraub, S. T., Levey, A. I., Chin, L.-S., and Li, L. (2005) Oxidative modifications and aggregation of Cu,-Zn-superoxide dismutase associated with Alzheimer and Parkinson diseases, *J. Biol. Chem. 280*, 11648−11655.
19. Bruijin, L. I., Houseweart, M. K., Kato, S., Anderson, K. L., Anderson, S. D., Ohama, E., Reaume, A. G., Scott, R. W., and Cleveland, D. W. (1998) Aggregation and motor neuron toxicity of an ALS-linked SOD1 mutant independent from wild-type SOD1, *Science 281*, 1851−1854.
20. Okado-Matsumoto, A., and Fridovich, I. (2002) Amyotrophic lateral sclerosis: a proposed mechanism, *Proc. Natl. Acad. Sci. U.S.A. 99*, 9010−9014.
21. Dobson, C. M. (2003) Protein folding and misfolding, *Nature 426*, 884−890.
22. Wang, J., Xu, G., Gonzales, V., Coonfielld, M., Fromholt, D., Copeland, N. G., Jenkins, N. A., and Borchelt, D. R. (2002) Fibrillar inclusions and motor neuron degeneration in transgenic mice expressing superoxide dismutase 1 with a disrupted copper-binding site, *Neurobiol. Dis. 10*, 128−138.
23. Johnston, J. A., Dalton, M. J., Gurney, M. E., and Kopito, R. R. (2000) Formation of high molecular weight complexes of mutant Cu,Zn-superoxide dismutase in a mouse model for familial amyotrophic lateral sclerosis, *Proc. Natl. Acad. Sci. U.S.A. 97*, 12571−12576.
24. Ross, C. A., and Poirier, M. A. (2005) Opinion: what is the role of protein aggregation in neurodegeneration?, *Nat. Rev. Mol. Cell Biol. 6*, 891−898.
25. Zhang, F., and Zhu, H. (2006) Intracellular conformational alterations of mutant SOD1 and the implications for fALS-associated SOD1 mutant induced motor neuron cell death, *Biochim. Biophys. Acta. 1760*, 404−414.
26. DiDonato, M., Craig, L., Huff, M. E., Thayer, M. M., Cardoso, R. M. F., Kassmann, C. J., Lo, T. P., Bruns, C. K., Powers, E. T., Kelly, J. W., Getzoff, E. D., and Tainer, J. A. (2003) ALS Mutants of human superoxide dismutase form fibrous aggregates via framework destabilization, *J. Mol. Biol. 332*, 601−615.
27. Khare, S. D., Caplow, M., and Dokholyan, N. V. (2004) The rate and equilibrium constants for a multistep reaction sequence for the aggregation of superoxide dismutase in amyotrophic lateral sclerosis, *Proc. Natl. Acad. Sci. U.S.A. 101*, 15094−15099.
28. Gaggelli, E., Kozlowski, H., Valennsin, D., and Valensin, G. (2006) Copper homeostasis and neurodegenerative disorders (Alzheimer's, Prion, and Parkinson's diseases and amyotrophic lateral sclerosis), *Chem. Rev. 106*, 1995−2044.
29. Jiang, W., Shen, T., Han, Y., Pan, Q., and Liu, C. (2006) Divalent-metal-dependent nucleolytic activity of Cu, Zn superoxide dismutase, *J. Biol. Inorg. Chem. 11*, 835−848.
30. Jiang, W., Han Y., Pan, Q., Shen, T., Liu, C. (2007) Roles of exogenous divalent metals in the nucleolytic activity of Cu,Zn superoxide dismutase, *J. Inorg. Biochem. 101*, 667−677.
31. Elam, J. S., Taylor, A. B., Strange, R., Antonyuk, S., Doucette, P. A., Rodriguez, J. A., Hasnain, S. S., Hayward, L. J., Valentine, J. S., Yeates, T. O., and Hart, P. J. (2003) Amyloid-like filaments and water-filled nanotubes formed by SOD1 mutant proteins linked to familial ALS, *Nat. Struct. Biol. 10*, 461−467.
32. Ray, S. S., Nowak, R. J., Strokovich, K., Brown, R. H., Jr., Walz, T., and Lansbury, P. T., Jr. (2004) An intersubunit disulfide bond prevents in vitro aggregation of a superoxide dismutase-1 mutant linked to familial amytrophic lateral sclerosis, *Biochemistry 43*, 4899−4905.
33. Chung, J., Xu, G., De Beus, M. D., Ryu, C. Y., Cho, K., and Colon, W. (2003) Cu/Zn superoxide dismutase can form pore-like structures, *Biophys. Res. Commun. 312*, 873−876.
34. Kurobe, N., Suzuki, F., Okajima, K., and Kato, K. (1990) Sensitive enzyme immunoassay for human Cu/Zn superoxide dismutase, *Clin. Chim. Acta 187*, 11−20.
35. Levy, Y., and Onuchic, J. N. (2006) Mechanisms of protein assembly: lessons from minimalist models, *Acc. Chem. Res. 39*, 135−142.
36. Wang, J., Xu, G., Li, H., Gonzales, V., Fromholt, D., Karch, C., Copeland, N. G., Jenkins, N. A., and Borchelt, D. R. (2005) Somatodendritic accumulation of misfolded SOD1-L126Z in motor neurons mediates degeneration: alphaB-crystallin modulates aggregation, *Hum. Mol. Genet. 14*, 2335−2347.
37. Liu, J., Lillo, C., Jonsson, A., Velde, C. V., Ward, C. M., Miller, T. M., Subramaniam, J. R., Rothstein, J. D., Marklund, S., Andersen, P. M., Brannstrom, T., Gredal, O., Wong, P. C., Williams, D. S., and Cleveland, D. W. (2004) Toxicity of familial ALS-linked SOD1 mutants from selective recruitment to spinal mitochondria, *Neuron 43*, 5−17.
38. Kim, Y.-J., Nakatomi, R., Akagi, T., Hashikawa, T., and Takahashi, R. (2005) Unsaturated fatty acids induce cytotoxic aggregate formation of amyotrophic lateral sclerosis-linked superoxide dismutase1 mutants, *J. Biol. Chem. 280*, 21515−21521.
39. Ginsberg, S. D., Galvin, J. E., Chiu, T. S., Lee, V. M., Masliah, E., and Trojanowski, J. Q. (1998) RNA sequestration to pathological lesions of neurodegenerative diseases, *Acta Neuropathol. 96*, 487−494.
40. Nandi, P. K., Leclerc, E., Nicole, J.-C., and Takahashi, M. (2002) DNA-induced partial unfolding of prion protein leads to its polymerisation to amyloid, *J. Mol. Biol. 322*, 153−161.
41. Cherny, D., Hoyer, W., Subramaniam, V., and Jovin, T. M. (2004) Double-stranded DNA stimulates the fibrillation of alpha-synuclein in vitro and is associated with the mature fibrils: an electron microscopy study, *J. Mol. Biol. 344*, 929−938.
42. Calamai, M., Kumita, J. R., Mifsud, J., Parrini, C., Ramazzotti, M., Ramponi, G., Taddei, N., Chiti, F., and Dobson, C. M. (2006) Nature and significance of the interactions between amyloid fibrils and biological polyelectrolytes, *Biochemistry 45*, 12806−12815.
43. Deleault, N. R., Lucassen, R. W., and Supattapone, S. (2003) RNA molecules stimulate prion protein conversion, *Nature 425*, 717−720.
44. Cordeiro, Y., Machado, F., Juliano, L., Juliano, M. A., Brentani, R. R., Foguel, D., and Silva, J. L. (2001) DNA converts cellular prion protein into the β-sheet conformation and inhibits prion peptide aggregation, *J. Biol. Chem. 276*, 49400−49409.
45. Lippard, S. J., Burger, A. B, Ugurbil, K., Pantoliano, M. W., and Valentine, J. S. (1977) Nuclear magnetic resonance and chemical modification studies of bovine erythrocyte superoxide dismutase: evidence for zinc-promoted organization of the active site structure, *Biochemistry 16*, 1136−1141.
46. McCord, J. M., and Fridovich, I. (1969) Superoxide dismutase. An enzymic function for erythrocuprein (hemocuprein), *J. Biol. Chem. 244*, 6049−6055.
47. Rakhit, R., Cunningham, P., Furtos-Matei, A., Dahan, S., Qi, X. F., Crow, J. P., Cashman, N. R., Kondejewski, L. H., and Chakrabartty, A. (2002) Oxidation-induced misfolding and aggregation of superoxide dismutase and its implications for amyotrophic lateral sclerosis, *J. Biol. Chem. 277*, 47551−47556.
48. Mastrangelo, I. A., Ahmed, M., Sato, T., Liu, W., Wang, C., Hough, P., and Smith, S. O. (2006) High-resolution atomic force microscopy of soluble Aβ42 oligomers, *J. Mol. Biol. 358*, 106−119.
49. Zhao, N. M., and Zhou, H. M. (2000) *Biophysics*, 1st ed., pp 73−98, China Higher Education Press, Beijing, and Springer-Verlag, Heidelberg.
50. Han, Y., Shen, T., Jiang, W., Xia, Q., and Liu, C. (2007) DNA cleavage mediated by copper superoxide dismutase via two patyways, *J. Inorg. Biochem. 101*, 214−224.
51. Haugland, R. P., Yue, S. T., Millard, P. J., and Roth, B. L. (1995) U.S. Patent 5,436,134.
52. Dong, J., Shokes, J. E., Scott, R. A., and Lynn, D. G. (2006) Modulating amyloid self-assembly and fibril morphology with Zn-(II), *J. Am. Chem. Soc. 128*, 3540−3542.
53. Pantoliano, M. W., McDonnell, P. J., and Valentine, J. S. (1979) Reversible loss of metal ions from the zinc binding site of copper-zinc superoxide dismutase. The low pH transition, *J. Am. Chem. Soc. 101*, 6454−6455.
54. Fee, J. A., and Phillips, W. D. (1975) The behavior of holo- and apo-forms of bovine superoxide dismutase at low pH, *Biochim. Biophys. Acta 412*, 26−38.
55. Liu, K., Cho, H. S., Lashuel, H. A., Kelly, J. W., and Wemmer, D. E. (2000) A glimpse of a possible amyloidogenic intermediate of transthyretin, *Nat. Struct. Biol. 9*, 754−757.
56. McParland, V. J., Kalverda, A. P., Homans, S. W., and Radford, S. E. (2002) Structural properties of an amyloid precursor of β2-microglobulin, *Nat. Struct. Biol. 9*, 326−331.

57. Swietnicki, W., Petersen, R., Gambetti, P., and Surewicz, W. K. (1997) pH-Dependent stability and conformation of the recombinant human prion protein PrP (90-231), *J. Biol. Chem. 272*, 27517−27520.
58. Blanch, E. W., Morozova-Roche, L. A., Cochran, D. A. E., Doig, A. J., Hecht, L., and Barron, L. D. (2000) Is Polyproline II Helix the Killer Conformation? A raman optical activity study of the amyloidogenic prefibrillar intermediate of human lysozyme, *J. Mol. Biol. 301*, 553−563.
59. Getzoff, E. D., Tainer, J. A., Weiner, P. K., Kollman, P. A., Richardson, J. S., and Richardson, D. C. (1983) Electrostatic recognition between superoxide and copper, zinc superoxide dismutase, *Nature 306*, 287−290.
60. Rousseau, F., Schymkowitz, J., and Serrano, L. (2006) Protein aggregation and amyloidosis: confusion of the kinds?, *Curr. Opin. Struct. Biol. 16*, 118−126.
61. Gamblin, T. C., King, M. E., Kuret, J., Berry, R. W., and Binder, L. I. (2000) Oxidative regulation of fatty acid-induced Tau polymerization, *Biochemistry 39*, 14203−14210.
62. Rangachari, V., Reed, D. K., Moore, B. D., and Rosenberry, T. L. (2006) Secondary structure and interfacial aggregation of amyloid-β (1-40) on sodium dodecyl sulfate micelles, *Biochemistry 45*, 8639−8648.
63. Kampers, T., Friedhoff, P., Biernat, J., Mandelkow, E. M., and Mandelkow, E. (1996) RNA stimulates aggregation of microtubule-associated protein tau into Alzheimer-like paired helical filaments, *FEBS Lett. 399*, 344−349.
64. Soto, C. (2003) Unfolding the role of protein misfolding in neurodegenerative diseases, *Nat. Rev. Neurosci. 4*, 49−60.
65. Nelson, R., and Eisenberg, D. (2006) Recent atomic models of amyloid fibril structure, *Curr. Opin. Struct. Biol. 16*, 260−265.
66. Tiwari, A., Xu, Z., and Hayward. L. J. (2006) Aberrantly increased hydrophobicity shared by mutants of Cu,Zn-superoxide dismutase in familial amyotrophic lateral sclerosis, *J. Biol. Chem. 280*, 29771−29779.
67. Arrasate, M., Mitra, S., Schweitzer, E. S., Segal, M. R., and Finkbeiner, S. (2004) Inclusion body formation reduces levels of mutant huntingtin and the risk of neuronal death, *Nature 431*, 805−810.
68. Taylor, J. P., Tanaka, F., Robitschek, J., Sandoval, C. M., Taye, A., Markovic-Plese, S., and Fischbeck, K. H. (2003) Aggresomes protect cells by enhancing the degradation of toxic polyglutamine-containing protein, *Hum. Mol. Genet. 12*, 749−757.
69. Bucciantini, M., Giannoni, E., Chiti, F., Baroni, F., Formigli, L., Zurdo, J., Taddei, N., Ramponi, G., Dobson, C. M., and Stefani, M. (2002) Inherent toxicity of aggregates implies a common mechanism for protein misfolding diseases, *Nature 416*, 507−511.
70. Kayed, R., Head, E., Thompson, J. L., McIntire, T. M., Milton, S. C., Cotman, C. W., and Glabe, C. G. (2003) Common structure of soluble amyloid oligomers implies common mechanism of pathogenesis, *Science 300*, 486−489.

BI062234M